Overtone Dissociation of Peroxynitric Acid (HO_2NO_2): Absorption Cross Sections and Photolysis Products†

Harald Stark,*,‡ Steven S. Brown, James B. Burkholder, Mattias Aldener,‡ Veronique Riffault,§ Tomasz Gierczak,|| and A. R. Ravishankara⊥

NOAA, Earth System Research Laboratory, 325 Broadway, Boulder, Colorado 80305

Received: March 14, 2008; Revised Manuscript Received: June 11, 2008

Band strengths for the second ($3\nu_{OH}$) and third ($4\nu_{OH}$) overtones of the OH stretch vibration of peroxynitric acid, HO_2NO_2 (PNA) in the gas-phase were measured using Cavity Ring-Down Spectroscopy (CRDS). Both OH overtone transitions show diffuse smoothly varying symmetrical absorption profiles without observable rotational structure. Integrated band strengths (base e) at 296 K were determined to be $S_{3\nu OH} = (5.7 \pm 1.1) \times 10^{-20}$ and $S_{4\nu OH} = (4.9 \pm 0.9) \times 10^{-21}$ cm^2 molecule^{-1} cm^{-1} with peak cross sections of $(8.8 \pm 1.7) \times 10^{-22}$ and $(7.0 \pm 1.3) \times 10^{-23}$ cm^2 molecule^{-1} at 10086.0 ± 0.2 cm^{-1} and 13095.8 ± 0.4 cm^{-1}, respectively, using PNA concentrations measured on line by Fourier-transform infrared and ultraviolet absorption spectroscopy. The quoted uncertainties are 2σ (95% confidence level) and include estimated systematic errors in the measurements. OH overtone spectra measured at lower temperature, 231 K, showed a narrowing of the $3_{\nu OH}$ band along with an increase in its peak absorption cross section, but no change in $S_{3\nu OH}$ to within the precision of the measurement (±9%). Measurement of a PNA action spectrum showed that HO_2 is produced from second overtone photodissociation. The action spectrum agreed with the CRDS absorption spectra. The PNA cross sections determined in this work for $3\nu_{OH}$ and $4\nu_{OH}$ will increase calculated atmospheric photolysis rates of PNA slightly.

1. Introduction

Odd hydrogen ($HO_x = OH + HO_2$) is one of the key radical families in the chemistry of the atmosphere. The most important mechanism for HO_x production in the troposphere and lower stratosphere is via a sequence of reactions involving O_3 photolysis and reaction of $O(^1D)$ with H_2O:

$$O_3 + h\nu(\lambda < 340\ \text{nm}) \rightarrow O(^1D) + O_2 \quad (1)$$

$$O(^1D) + H_2O \rightarrow OH + OH \quad (2)$$

The actinic flux in the UV wavelength range where ozone photolysis produces $O(^1D)$ decreases significantly at high solar zenith angles (SZA), with a consequent reduction in the OH radical production rate. At high SZA (e.g., high latitude winter and periods near dawn and dusk), other photochemical HO_x production pathways that occur at longer wavelengths become more important because of the relatively larger attenuation of shorter wavelengths through the longer atmospheric paths. One such process is HO_x production via overtone excitation of peroxynitric acid (PNA, HO_2NO_2).[1]

Direct overtone photodissociation (DOP) involves photolytic excitation into a vibrational overtone at visible or near-infrared wavelengths. Intramolecular vibrational energy redistribution (IVR) may then lead to dissociation of the molecule provided it contains a chemical bond weaker than the overtone excitation energy. Overtone transitions in the OH stretch vibration with 2−5 quanta of vibrational energy have been reported for molecules that include H_2O_2, HNO_3, HONO, HOCl, HOBr, and HO_2NO_2.[1] The overtone transitions for many of these molecules are strong enough to yield an atmospherically relevant photolysis rate (*j*-value) at high SZA. In this study, we have measured the OH overtone absorption cross sections of peroxynitric acid. The two quantities needed for an evaluation of PNA overtone photolysis in the atmosphere are the absorption cross section for the transition and the quantum yield for dissociation. The relative yields for different product channels are also of importance for atmospheric HO_x production from PNA overtone photolysis. Here we show that HO_2 is produced by absorption around 990 nm, i.e., the second OH overtone band ($3_{\nu OH}$) of PNA.

Peroxynitric acid is formed in the atmosphere by reaction of HO_2 with NO_2. Because it is unstable with respect to thermal decomposition, it is generally most important in cold environments (i.e., high altitude and/or polar regions), where it serves as a reservoir species for both the HO_x and NO_x (=NO + NO_2) families. Its importance in this role depends on its total atmospheric loss rate, which is due to thermal decomposition, reaction with hydroxyl radical (OH) and photolysis:

$$HO_2 + NO_2 \rightarrow HO_2NO_2\ (\text{PNA}) \quad (3)$$

$$HO_2NO_2 + M \rightarrow HO_2 + NO_2 \quad (4)$$

$$HO_2NO_2 + OH \rightarrow H_2O + O_2 + NO_2 \quad (5)$$

$$HO_2NO_2 + h\nu \rightarrow HO_2 + NO_2\ (\lambda_T = 1180\ \text{nm}) \quad (6a)$$

$$\rightarrow OH + M + NO_3\ (\lambda_T = 730\ \text{nm}) \quad (6b)$$

* To whom correspondence should be addressed. E-mail: harald.stark@noaa.gov.

† Part of the "Stephen R. Leone Festschrift".

‡ Also affiliated with the Cooperative Institute for Research in Environmental Sciences, University of Colorado, Boulder, Colorado 80309.

§ Permanent address: Ecole des Mines de Douai - Département Chimie et Environnement, 941 rue Charles Bourseul, BP 10838, 59508 Douai cedex, France.

|| Permanent address: Department of Chemistry, Warsaw University, ul. Zwirki i Wigury 101, 02-089, Warsaw, Poland.

⊥ Also affiliated with the Department of Chemistry and Biochemistry, University of Colorado, Boulder, Colorado 80309.

10.1021/jp802259z CCC: $40.75
Published on Web 08/27/2008

$$\rightarrow \text{HONO} + O_2(^1\Sigma)(\lambda_T = 1740\ \text{nm}) \quad (6c)$$

$$\rightarrow \text{HONO} + O_2(^3\Sigma)(\lambda_T = 1240\ \text{nm}) \quad (6d)$$

where λ_T is the photolysis threshold wavelength calculated from heats of formation at 298 K.[2] A recent theoretical investigation[3] of the overtone photodissociation of PNA has shown that $HO_2 + NO_2$ (6a) is the only photolytically available product channel from the first, second, and third overtone without intersystem crossing into the triplet state channel. There have been two recent experimental studies that reported the PNA thermal decomposition rate coefficient[4] and the rate coefficient and product yields for the PNA + OH reaction.[5] These reaction rate coefficients, together with typical conditions found in the upper troposphere - lower stratosphere (UT-LS) (7−9 km, ∼240 K, 1×10^6 molecules cm^{-3} OH)[6] result in lifetimes of PNA of 55 and 60 h with respect to thermal dissociation and OH reaction, respectively.

Direct overtone photodissociation is particularly important to the atmospheric chemistry of PNA because its threshold to yield HO_2 and NO_2 is low (24 ± 1 kcal mol^{-1}) and is accessible via excitation into the second and higher overtones in the visible or near-IR spectral regions. Indeed, the calculated lifetime of PNA with respect to photolysis, including DOP, is about half of that due to thermal dissociation and reaction with OH for the UT-LS conditions noted above.

The first overtone (centered at 1440 nm) lies just below the dissociation threshold (24 kcal mol^{-1}) and is partially available for DOP with a temperature-dependent quantum yield below unity. Direct overtone photolysis is possible because of the additional thermal energy available in the molecule which, in combination with the photon energy, allows dissociation with a quantum yield depending on temperature. The first three overtones dominate DOP for PNA since cross sections for higher overtones decrease by about an order of magnitude for successive vibrational quanta.[7] Zhang et al.[8] recently used UV absorption and direct IR absorption to measure band strengths (i.e., integrated cross sections) for the second ($3\nu_{OH}$) and third ($4\nu_{OH}$) overtone of PNA to be $(3.8 \pm 1.1) \times 10^{-20}$ and $(3.0 \pm 1.8) \times 10^{-21}$ cm^2 $molecule^{-1}$ cm^{-1}, respectively. Roehl et al. [9] indirectly measured the HO_2 photoproduct (by reacting HO_2 with NO to form OH, which was then detected using laser induced fluorescence) from the photolysis of PNA at near-infrared wavelengths (i.e., action spectroscopy). They concluded that the first overtone ($2\nu_{OH}$) of PNA makes the largest contribution to the total PNA DOP rate. They reported an integrated absorption cross section of $S_{2\nu OH} = (9.5 \pm 1.9) \times 10^{-19}$ cm^2 $molecule^{-1}$ cm^{-1} based on measurements made relative to the fundamental and second overtone bands and a pressure-independent photolysis quantum yield for the first overtone of 0.14 at 240 K assuming unit quantum yield for HO_2 production from second overtone photolysis. They calculated a PNA DOP rate J_{DOP}, including 2, 3, and $4\nu_{OH}$ of 8.3×10^{-6} s^{-1} under clear-sky conditions. Matthews et al.[10] used double-resonance spectroscopy to investigate the first overtone transition of PNA. They reported a quantum yield of 0.3 at 298 K, which compares well to the value of 0.27 measured by Roehl et al.[9] They also confirmed the lack of pressure dependence in the PNA quantum yield indicating that only additional thermal energy in the ground state, and not collisional stabilization of the excited state, lead to dissociation. A theoretical study by Matthews et al.[11] reported values for the transition frequencies and band strengths for the OH-stretch vibration from the fundamental to the fifth overtone. The band strengths for the first and second overtones of calculations and measurements were confirmed to within 15% whereas the calculated band strength for the third overtone was 40% smaller.

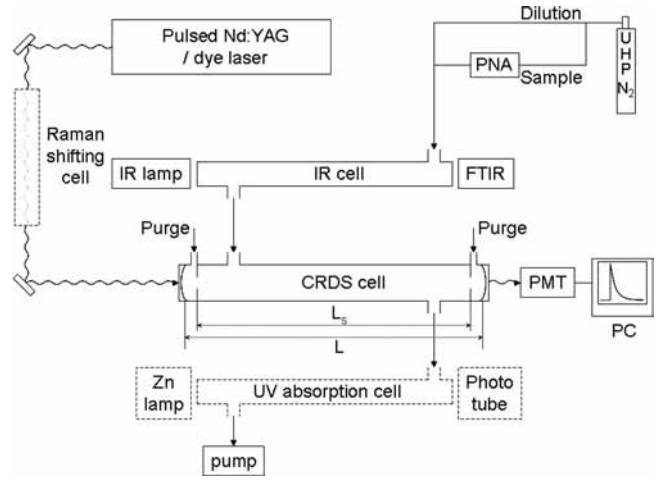

Figure 1. Experimental setup: straight lines with arrows indicate flow direction, wavy lines indicate laser light beams; dashed section shows the UV absorption cell, which was used in a limited number of experiments.

Several recent measurements of PNA in the free troposphere and in the Arctic, as well as photochemical models of partitioning among various reactive nitrogen species, support the conclusion that near-infrared photolysis of PNA is significant at high solar zenith angles and cold temperatures. Wennberg et al.[12] proposed such a mechanism based on comparisons of modeled to measured HO_x levels in the high latitude lower stratosphere. Salawitch et al.[6] later showed that near IR photolysis can be the dominant PNA loss process under these conditions, which was supported by a comparison between balloon observations and a 3D global modeling study.[13] More recent measurements of PNA and related species (HO_2, NO_2, OH) at high altitudes[14–16] and in polar regions[17–19] have confirmed these results and have shown that near-infrared photolysis needs to be included in order to correctly account for the reactive nitrogen partitioning in these regions.

In this paper, we provide measurements of the absorption cross sections for PNA in its second ($3\nu_{OH}$) and third ($4\nu_{OH}$) overtone bands. These measurements are based on cavity ring-down spectroscopy (CRDS), a high sensitivity, direct absorption spectroscopic technique that is particularly applicable to the precise determination of weak absorptions. This experimental approach is a complimentary method to the direct IR absorption and HO_2 action spectroscopy of Roehl et al.[9] and Zhang et al.[8] and double-resonance spectroscopy of Matthews et al.[10] used to study the first, second and third overtones of PNA. We also provide information on the production of HO_2 in the overtone photodissociation of PNA around 990 nm via HO_2 action spectroscopy.

2. Experimental Details

Absorption Cross Section Measurements. Here, we describe the experimental setup and methods used to measure the second and third overtone of PNA. A combination of three spectroscopic methods including cavity ring-down, Fourier-transform infrared (FTIR) and UV absorption spectroscopy were used. The experimental apparatus consisted of two or three absorption cells in series with respect to the sample flow as shown in Figure 1 and was used to measure absolute intensities of PNA overtone absorption spectra. The absorption cells were made of glass, and all transfer lines and fittings were made of

Teflon (PFA). A flow of dry nitrogen passing through a flask containing liquid PNA (along with impurities of HNO_3, H_2O_2, and NO_2) at −17 °C was the source for gaseous PNA. The PNA concentration was measured by its mid-infrared absorbance with an FTIR spectrometer. To measure the much weaker overtone absorption bands of PNA in the visible and near-infrared wavelength region, we used pulsed Cavity Ring-Down Spectroscopy (CRDS). For recording HNO_3 and H_2O_2 near-IR reference spectra, we used CRDS for absorption measurements and either UV absorption from a zinc lamp (Figure 1) or the FTIR spectrometer for determining concentrations of HNO_3 and H_2O_2. In the following, we give a brief description of the experimental technique and the apparatus and outline the features specific to the present measurements.

The CRDS method allows sensitive measurement of weak optical transitions by measuring the time constants, τ, for the single exponential decay of light intensity from an optical cavity with and without absorbers present. The absorption coefficient, α, can be directly calculated from the measurements by

$$\alpha(\mathrm{cm}^{-1}) = N\sigma(\lambda) = \frac{1}{c}\frac{L}{L_S}\cdot\left(\frac{1}{\tau}-\frac{1}{\tau_0}\right) \qquad (7)$$

with N, number density of the absorber (molecule cm^{-3}), $\sigma(\lambda)$, absorption cross section at wavelength λ (cm^2 $molecule^{-1}$), c, speed of light (2.998×10^4 cm μs^{-1}), L, optical cavity length (cm), L_S, length over which absorber is present (cm), τ, ring-down time with absorber present (μs), and τ_0, empty cavity ring-down time (μs). Absorption coefficients on the order of $10^{-9}cm^{-1}$ and lower have been measured quantitatively with this experimental setup.[20] The basics of the CRDS experimental setup have been described elsewhere.[20,21]

A Nd:YAG (532 nm) pumped dye laser generated 6−8 ns laser pulses at wavelengths between 720 and 780 nm, which encompassed the third PNA overtone centered at 762 nm. For the second overtone, near-infrared light from 975 to 1010 nm was generated by Raman-shifting (1st Stokes) visible light between 694 and 711 nm in a high pressure H_2 cell. The near-IR pulses were separated from other wavelengths by dichroic mirrors, passed through a telescope to approximately match the laser to low-order transverse electric modes of the cavity and coupled into the ring-down cell directly through the front mirror. We used two different cavity lengths (L), 93 and 187.6 cm. The reflectivity of the cavity mirrors changed slightly from 99.9979% to 99.9981% in the wavelength region between 758 and 770 nm and decreased from 99.997% to 99.987% between 983 and 1011 nm, which resulted in empty cavity ring-down times between 145 and 160 μs for the visible wavelengths in the short cavity and between 320 and 48 μs for near-IR wavelengths in the long cavity. The temporal profiles of the light intensity exiting the rear mirror of the cavity were detected using a photomultiplier and digitized by an oscilloscope card in a computer, where they were fit to single exponential decays. Average ring-down times were calculated by fitting individual traces and averaging their ring-down times. Absorption coefficients, α, were calculated from eq 7, with τ_0 and τ measured in the same bath gas flow with the PNA sample absent and present, respectively. We recorded reference spectra for HNO_3, H_2O_2, and NO_2 in the visible and near-IR by flowing pure samples of these compounds through the same apparatus used for the PNA measurements. These reference spectra were used to subtract HNO_3, H_2O_2, and NO_2 from each measured spectrum.

Purge flows in front of the CRDS mirrors were used to protect them from exposure to the reactive gases flowing through the cell and to keep them clean. This resulted in a shorter effective path length (L_s) than the cell length. The geometrical distance between the ends of the purge volumes agreed well with optical calibration measurements made using ozone absorption and was independent of flow rates. The path lengths were determined by flowing a known concentration of ozone (determined by UV absorption at 253.85 nm in a separate cell) through the ringdown cell and measuring its absorption either by CRDS at 680 nm (Chappuis band) or by direct UV absorption at 253.85 nm (Hartley band) using quartz windows in place of the CRDS mirrors. The ratio L/L_s was determined to be (1.30 ± 0.04) and (1.10 ± 0.03) for the 93 and 187.6 cm mirror distances, respectively.

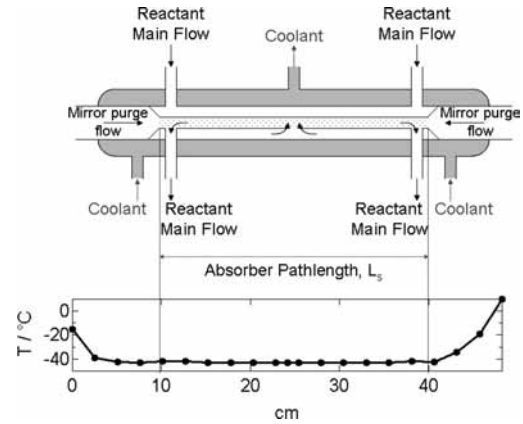

Figure 2. Flow directions and temperature profile in temperature-controlled CRDS cell; note that the temperature profile throughout absorber path length is constant to within 2 K.

PNA concentrations were measured using a Fourier-transform infrared spectrometer (FTIR). Because of the difference in sensitivity between the FTIR and CRDS measurements, it was generally necessary to perform the FTIR measurements in a more concentrated flow that was then diluted using calibrated gas flows to a lower concentration prior to entering the CRDS cell.

Low temperature CRDS measurements were made using the cell shown in Figure 2, which was designed for effective precooling of the gases before entering the CRDS optical path. The cell was inserted midway between the cavity mirrors using copper tubing as a spacer to fill the distance of 187.6 cm between the mirrors. The cell was 56 cm in length, and the jacketed section was 45 cm long. The effective optical path length of this cell was determined by measuring absorption from a known concentration of ozone as described above and found to be 27.4 ± 0.5 cm independent of temperature and the range of flow rates used in the PNA measurements. This path length was significantly shorter than the jacketed region because of the location of the inlet and outlet used to ensure a homogeneous temperature profile. We confirmed that the temperature profile was homogeneous to within 2 K over the entire effective path length by measuring the temperature profile under the experimental pressure and flow conditions (see Figure 2). Low temperature measurements could only be performed at pressures below 100 Torr to avoid large gas density fluctuations at the mixing zone between purge flows (warm) and absorber flows (cold). At higher pressures, the empty cavity ringdown time changed significantly (by up to 50% at 600 Torr) and irreproducibly when changing the temperature. Below 100 Torr, the maximum change at different pressures of the ring-down time was on the order of 1 μs, which was small enough to allow quantitative absorption measurements.

A major difficulty in measuring the overtone absorption cross sections of PNA is the accurate determination of the gas phase

PNA concentration. PNA is thermally unstable and may decompose via either homogeneous or heterogeneous processes during its residence in the flow system. The loss of PNA on the flow-tube surfaces was determined in a limited number of experiments in which the PNA concentration in both cells was measured by reversing the gas flow. The concentration determined in the FTIR cell did not change within the precision of the measurement of ±5% after reversing the flow. Flow rates through the flask were in the range from 60 to 400 standard cubic cm per minute (sccm). These flows, together with dilution flows of up to 2000 sccm, led to residence times through the FTIR/CRDS(/UV) absorption cells of less than 30 s.

Nitric acid (HNO_3) and hydrogen peroxide (H_2O_2) were the most significant impurities in the PNA sample. To separate their contribution from that of PNA in the FTIR measurements, we obtained FTIR reference spectra from 700 to 4000 cm^{-1} of PNA, HNO_3, and H_2O_2 by relative UV/IR measurements using a diode-array spectrometer and the FTIR. The band strengths of our reference spectra for these impurities agreed with previous measurements.[22–24] We used literature UV PNA spectra [25,26] for the concentration measurements and compared our results of 2.2×10^{-17} cm^2 $molecule^{-1}$ cm^{-1} for the integrated cross section at 803 cm^{-1} (scissor mode of the nitrate group) with previous studies.[25,27,28] The agreement between our measurements and previous measurements was better than 10%. These band strength measurements also support our contention of a small loss of PNA in the flow through the apparatus.

For quantifying concentrations from the FTIR data, we developed a spectral fitting routine similar to the numerical methods used for deconvoluting spectra from differential optical absorption spectroscopy (DOAS) measurements.[29] PNA concentrations in the CRDS cell ranged between 1×10^{14} and 5×10^{15} molecules cm^{-3}. PNA was synthesized by adding nitronium tetrafluoroborate (NO_2BF_4) to concentrated hydrogen peroxide (≥95 wt %) in a dry nitrogen atmosphere, following the prescription of Kenley et al.[30] By-products of this synthesis include SiF_4, HNO_3, H_2O_2, NO_2, and H_2O, each of which was identified in the FTIR spectrum.

The inert gas in all experiments was ultra high purity nitrogen (UHP N_2). Pressures were measured in the IR, CRDS, and UV absorption cells using capacitance manometers and ranged between 10 and 60 Torr. The room temperature measurements were conducted at 296 ± 1 K; low temperature measurements were made at 231 ± 1 K. Gas flows were measured using calibrated electronic mass flow meters.

Measurements of HO_2 Production in the $3\nu_{OH}$ Overtone Photodissociation of PNA. In a second set of experiments, we used action spectroscopy to study the photolysis products from excitation of the second PNA overtone. The pulsed-photolysis pulsed laser induced fluorescence (LIF) apparatus, which has been used extensively for measuring rate coefficients of OH reactions in our laboratory, was used to investigate the production of HO_2 in the photodissociation of PNA at 298 K. Details of the LIF apparatus are given elsewhere.[5] The laser used for photolysis was the same as that used for the CRDS overtone cross section measurements. OH radicals were detected via pulsed laser induced fluorescence as a function of time after photolysis to measure temporal profiles of OH.

First, a mixture of PNA and N_2 was photolyzed around 990 nm. The amount of OH produced in these measurements was below the detection limit for OH. Next, mixtures of PNA ($0.1-1.6 \times 10^{15}$ molecules cm^{-3}), NO ($0.2-1.1 \times 10^{15}$ molecules cm^{-3}), and N_2 (total pressure 49−51 Torr) were photolyzed. In these experiments, HO_2 was produced from the overtone photodissociation,

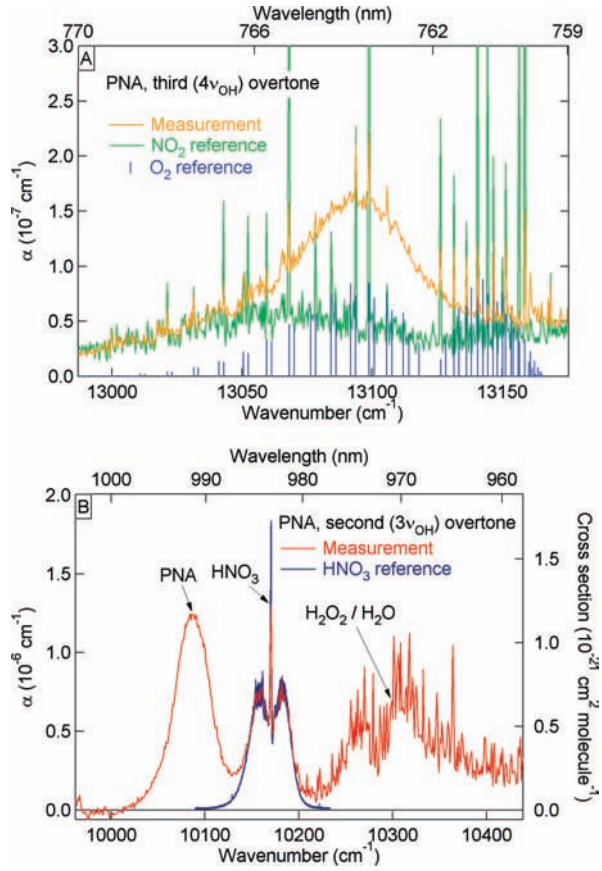

Figure 3. Cavity ring-down absorption coefficients α, vs wavenumber (bottom) and wavelength (top); panel A: third ($4\nu_{OH}$) overtone region of PNA with reference spectra of O_2 and NO_2; panel B: second ($3\nu_{OH}$) overtone region of PNA, HNO_3, and H_2O_2 with reference spectrum of HNO_3.

$$PNA + h\nu \rightarrow HO_2 + NO_2 \quad (8)$$

HO_2 radicals reacted with NO to produce OH within about 100 μs.

$$HO_2 + NO \rightarrow OH + NO_2 \quad (9)$$

$k = 8 \times 10^{-12}$ cm^3 $molecule^{-1}$ s^{-1} (from Sander et al.[2])

Biexponential profiles were fitted to the temporal profiles of OH and yielded the value of HO_2 at time zero (directly after photolysis) and the loss rate of OH, mainly due to reaction with PNA (reaction 5, see above). The experiments with NO were carried out at discrete wavelengths between 983 and 996 nm and covered the entire second overtone band of PNA. The analysis of the experiments with and without NO present were used to investigate the relative yield of HO_2 vs OH from second overtone photodissociation of PNA. The analysis also yielded an action spectrum of this overtone transition that could be compared to the CRDS absorption spectrum.

3. Results and Discussion

Figure 3 shows absorption coefficients, α, measured by CRDS for the wavelength regions of the two overtones (759−770 nm for the third and 960−1000 nm for the second overtone) along with reference spectra for the impurities that were present in significant amounts. For the third overtone, absorption by NO_2 and O_2 were the largest contributions to the absorption spectra,

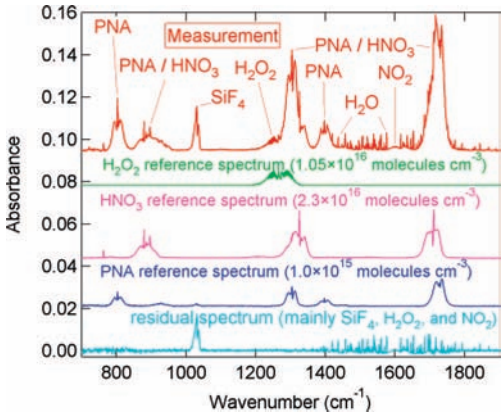

Figure 4. FTIR spectra showing the components of the gas phase PNA sample mixtures (top) with reference spectra (from top to bottom) of H_2O_2, HNO_3, and PNA; traces are offset for clarity; bottom trace shows residuals after spectral subtraction of PNA, HNO_3, and H_2O_2.

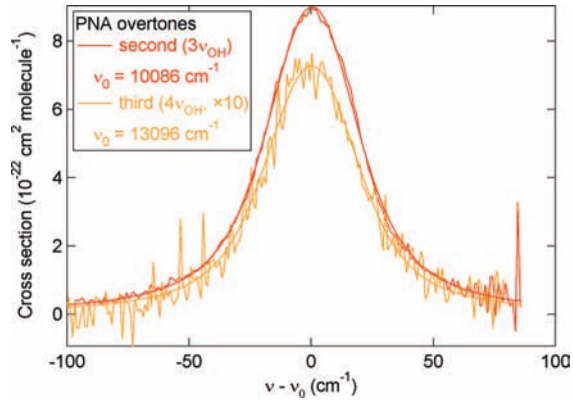

Figure 5. Spectra of cross section vs frequency shift from peak center ($\nu-\nu_0$) for the second ($3\nu_{OH}$, red) and third ($4\nu_{OH}$, orange) overtone O−H-stretch vibration of PNA; reference spectra of impurities (HNO_3, O_2, and NO_2) were removed; solid lines show Voigt fits for $3\nu_{OH}$ and $4\nu_{OH}$, respectively.

aside from PNA. The agreement between observed and literature O_2 line positions of the O_2 *A*-band is apparent, although there are missing O_2 lines in the measurement spectrum due to the dye laser step size exceeding the O_2 linewidths. The O_2 line positions were used to calibrate the wavelength of the dye laser to an accuracy of ± 0.4 cm^{-1}. The O_2 lines were removed from the spectra for determining the PNA integrated cross sections by interpolating between points adjacent to the O_2 lines. NO_2 has a very irregularly structured spectrum in this region and subtraction of the NO_2 reference spectrum was less accurate. Spectral interference from NO_2 therefore resulted in a noisier PNA residual spectrum for the third overtone band.

The spectrum shown in Figure 3B spans the wavelength region of the second overtones of PNA, HNO_3, and H_2O_2. HNO_3 had the largest overlapping absorption with PNA and its contribution to the measured spectra was subtracted using reference spectra. It was not necessary to subtract H_2O_2 from the spectra since its overlap with the PNA spectrum was negligible. The subtraction of reference spectra increased the uncertainty in both PNA overtone spectra. However, this additional uncertainty was a negligible contribution (<0.1%) to the band strengths.

Figure 4 shows a typical mid-infrared FTIR spectrum with identified transitions of PNA, SiF_4, HNO_3, H_2O_2, NO_2, and H_2O. Also included in the figure are reference spectra for HNO_3 and H_2O_2 that were used for spectral fitting (see previous section for a description) and concentration determination. Quantification of H_2O, NO_2 and SiF_4 was unnecessary. Regions with possible interferences from H_2O, NO_2, and SiF_4 were excluded from the fitting of the infrared spectrum and determination of the PNA concentration. The bottom trace in Figure 4 shows the residual after the spectral fitting, which does not show signatures of PNA, HNO_3, or H_2O_2. The remaining features are attributable to SiF_4, H_2O, and NO_2. We analyzed all FTIR spectra in this way and retrieved concentrations for PNA, HNO_3, and H_2O_2. The precision of the PNA concentrations from this method is better than 5%, not including systematic uncertainties from the reference spectrum.

Figure 5 shows averaged CRDS spectra of the second and third (scaled by a factor of 10) PNA overtone after subtracting reference spectra of HNO_3, NO_2 and O_2. Both spectra exhibit smoothly varying envelopes without observable rotational structure within the laser line width of 0.05 cm^{-1}. However, individual lines from imperfect subtraction of the impurities spectra are visible. The absorption spectra are symmetric and Voigt profiles fit the entire rovibrational bands very well. Voigt fits were consequently used to determine parameters such as peak and integrated cross sections, peak positions and widths of the overtone bands. We used the Voigt fit results rather than the measured spectra directly for three reasons. First, the fits served to reduce uncertainty due to slight fluctuations in the baseline and reduced the frequency with which zero determinations (by turning off the PNA flow) were necessary. Second, a Voigt fit reduces uncertainties in parameters such as peak intensity and bandwidth by reducing contributions from outliers that remain in the spectra due to incomplete removal of impurity reference spectra. Third, the fit profile gives an estimate of contributions from the wings of the spectra where the overtone absorption cross sections are small and difficult to measure accurately. However, the small cross sections in the wings of the spectra are important. For example, approximately 12% of the total band strength (determined from the Voigt fits) originate from sections of the spectra below 5% of the peak intensity. To ensure that the Voigt fits correctly represented the intensities in the wings, high-precision measurements of the absorption cross section were achieved in several measurements by using longer averaging at fixed wavelengths. The higher-precision measurements confirmed the intensity predicted by the Voigt fits. Measurement of the entire overtone spectrum at higher precision was not possible due to the gradual fluctuations in the PNA concentrations.

A disadvantage arising from fitting to a profile with a functional form is that it does not necessarily represent the actual shape of the PNA absorption bands, which are the sum of a series of overlapping rovibrational lines that do not necessarily have regular spacing or a symmetric envelope. Analysis of the shapes of the two overtone bands measured in this work were, however, accurately reproduced using a Voigt profile.

We calculated averages of the fitting parameters obtained from all measured spectra; the results are given in Table 1. The stated errors given in Table 1 are 2σ standard deviations of the mean based on 24 measurements of $3\nu_{OH}$ and 6 measurements of $4\nu_{OH}$.

We also conducted cross section measurements of the second overtone at 231 K. Figure 6 shows a comparison of the low- and room temperature measurements and table 1 gives the parameters from Voigt profile fits to these bands. A significant narrowing of the bandwidth (fwhm decreased by 21%) as well as an increase in peak cross section by 28% is apparent in the lower temperature spectrum. The integrated cross sections, however, are the same within the ranges of the individual

TABLE 1: Parameters from Voigt Profile Fits to the Second ($3\nu_{OH}$) and Third ($4\nu_{OH}$) OH-Stretch Overtone Bands of PNA[a]

	$4\nu_{OH}$ (298 K)	$3\nu_{OH}$ (298 K)	$3\nu_{OH}$ (231 K)
$\tilde{\nu}_{peak}$ (cm^{-1})	13095.8 ± 0.4	10086.0 ± 0.2	10088.0 ± 0.2
integral (10^{-20} cm^2 cm^{-1})	0.492 ± 0.047	5.7 ± 0.3	5.5 ± 0.9
fwhm (cm^{-1})	48.4 ± 1.4	44.6 ± 0.6	37.6 ± 3.8
σ_{peak} (10^{-22} cm^2)	0.70 ± 0.03	8.8 ± 1.1	11.3 ± 1.3

[a] Erors are 2σ (95% confidence level) of the measurement precision.

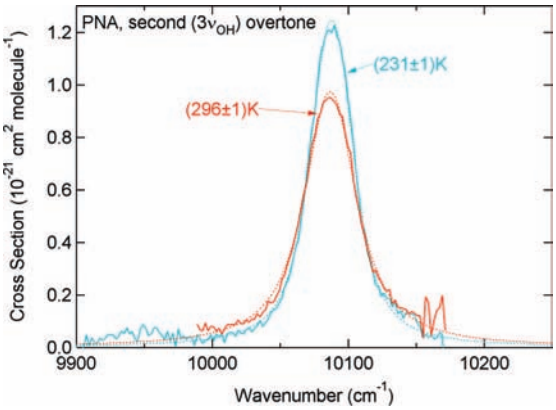

Figure 6. Temperature dependence of the second ($3\nu_{OH}$) overtone transition of PNA; 298 K (solid red: measurements, dotted red: Voigt fit) and 231 K (solid light blue: measurements, dashed light blue: Voigt fit); note the narrowing of the band at the lower temperature, without a change in the integrated band strength.

measurements. This suggests either that there is only a single PNA conformer populated at room temperature, or that there are one or more conformers with similar transition intensities. Some previous theoretical and spectroscopic studies have concluded that only one ground-state conformer exists.[31–33] The calculated geometry of the OONO skeleton is planar, while the O−H bond is nearly orthogonal to this plane.[34] A recent paper by Matthews et al.[11] calculated 5 stable ground-state conformers with 3 being 0.3 kcal mol^{-1} above the global minimum energy. This energy difference would result in a relative change in populations of up to 16% between 231 and 298 K. The observation of a temperature-independent integrated cross section in combination with the different ground-state conformers indicates that the band strengths of the different conformers are similar.

The potential systematic errors that may influence the accuracies of the cross section measurements from our work include uncertainties in flow meter calibrations (5%), IR spectral fitting of PNA (5%), and the determination of the ratio L/L_s (3%). Additional sources of error in the integrated cross section result from uncertainties in subtraction of the reference spectra of HNO_3, H_2O_2, and NO_2 (5%). For the most part of the PNA overtone spectra, the impurities did not contribute to the measured cross sections because their absorptions occur at wavelengths distinctly different from that by PNA. A quadratic combination of the estimated systematic errors leads to an overall uncertainty of 9%, which is in the range of the standard deviations obtained from replicate measurements (see Table 1). Additionally, we estimate the uncertainty of the mid-IR PNA cross section used in the FTIR measurements to be on the order of 10%, which increases the total uncertainty of the measurements to 19%. If the mid-IR cross section of PNA of 2.2×10^{-17} cm^2 $molecule^{-1}$ cm^{-1} is ever revised in the future, the results for the overtone cross sections and error limits reported here can be scaled accordingly.

TABLE 2: Integrated Band Strengths of OH Stretch Vibrations in HO_2NO_2 (PNA)

	band strength (10^{-20} cm^2 $molecule^{-1}$ cm^{-1})	ref
$1\nu_{OH}$	610 ± 73	May and Friedl (1993)[35]
(fundamental)	720 ± 140	Roehl et al. (2002)[9]
	740	Matthews et al. (2004)[11]
$2\nu_{OH}$	95 ± 19	Roehl et al. (2002)[9]
(first overtone)	90.3	Matthews et al. (2004)[11]
$3\nu_{OH}$	3.3 ± 0.7	Roehl et al. (2002)[9]
(second overtone)	3.8 ± 1.1	Zhang et al. (2000)[8]
	5.7 ± 1.1	this work (2008)
	3.61	Matthews et al. (2004)[11]
$4\nu_{OH}$	0.30 ± 0.18	Zhang et al. (2000)[8]
(third overtone)	0.49 ± 0.09	This work (2008)
	0.179	Matthews et al. (2004)[11]
$5\nu_{OH}$ (fourth overtone)	0.0156	Matthews et al. (2004)[11]

Table 2 compares our results with previous measurements and calculations of ν_{OH} fundamentals and overtones for PNA. The results obtained from this work for the second and third overtone are significantly larger than previous measurements by Zhang et al.[8] The results by Zhang et al. for the second overtone were later re-evaluated by the same group using absorption measurements relative to the fundamental.[9] The re-evaluation resulted in a reduction of the intensity of the second overtone ($3\nu_{OH}$) by 13%. The values from this work for the second and third overtone are 73% and 63% larger than these revised measurements. We note that the differences between the measurements from this study and the previous experimental study by Zhang et al.[8] agree within the combined error limits of both studies. However, after re-evaluation of the Zhang et al. values by Roehl et al.,[9] the results for the second overtone from this work lie outside the combined error limits. The Roehl et al. study[9] also presented results for the first overtone, which are included in Table 2. Also included in this table are results from a recent theoretical study by Matthews et.al.[11] The values from our work are outside the error limits and 58% and 170% larger than the results from the theoretical study for the second and third overtone, respectively.

Production of HO_2 from PNA Overtone Photodissociation. The temporal profiles of OH showed that there was little OH (<10%) produced upon photolysis of PNA and the OH measured was from the reaction of HO_2 with NO. Comparison of the peak OH values in the presence of NO to the OH upper limit without NO results in a relative yield of HO_2 to OH from second overtone photolysis of PNA of 100 ± 10%. The uncertainty is 2σ of the average measurement uncertainty of the experiment without NO present.

Figure 7 shows an action spectrum of HO_2 of the PNA $3_{\nu OH}$ overtone band (normalized to the peak value at 991.5 nm) as a function of wavelength between 983 and 996 nm superimposed on the combined absorption by HNO_3 and PNA and the absorption spectrum of PNA (same measurement as shown in Figures 3 and 5) that take place in this region. Absolute HO_2 concentrations were not determined.

A few findings are clear. First, the relative HO_2 yield largely follows the PNA absorption feature, showing that the HO_2 yield is the same at various wavelengths with the exception of wavelengths below 990 nm, where the HO_2 action spectrum is slightly higher than the absorption feature measured by CRDS. This deviation can be attributed to fluctuations in the photolysis laser fluence. The uncertainties in these measurements are large due to low OH signal levels, but the trend is clear. Second, the measurements suggest that no HO_2 or OH is produced from HNO_3 absorption in the second overtone region. Third, not shown in the figure, but evident was that no OH is produced

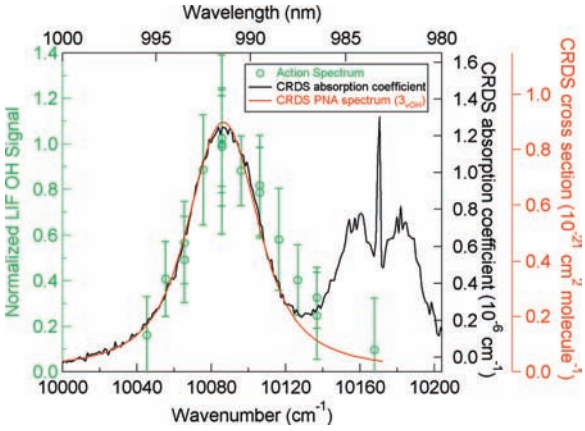

Figure 7. Comparison of PNA action spectrum (circles) with CRDS absorption coefficient (black) and the PNA $3_{\nu OH}$ cross section spectrum (red). The PNA action spectrum was measured by indirect HO_2 detection via laser induced fluorescence of OH produced from the $HO_2 + NO \rightarrow OH + NO_2$ reaction. The CRDS spectra are the same as the ones shown in Figures 3 and 5. Note that the CRDS absorption coefficient was not corrected for any baseline drifts and therefore has a slight vertical offset.

by the absorption in this region indicating that OH production is energetically not possible at these wavelengths.

We could not place these relative yields on an absolute basis to calculate quantum yields. The main difficulty was in producing a spatially uniform laser beam at around 990 nm. However, production of such a beam would entail a major loss in fluence and prevented us from pursuing this further. Because of these difficulties, we can not rule out production of HONO from PNA photolysis.

A recent study by Roehl et al.[9] used the same technique of HO_2 action spectroscopy of PNA. Our result of zero OH production from the second PNA overtone band agrees with results from the Roehl et al. study.

4. Atmospheric Implications

There are two recent modeling studies of the atmospheric fate of PNA that include visible and near-IR photolysis using the results from Roehl et al.[9] for the overtone band strengths.[6,13] Both models achieve a much better level of agreement between calculated and measured PNA and HO_x in the upper troposphere and stratosphere than obtained in previous model calculations not including direct overtone photolysis. However, both models still slightly underestimate HO_x. The results for band strengths of the second and third overtones from our work, combined with the solar flux values given in Roehl et al.[9] increase the overall PNA photolysis rate by 11%. The difference between our results based on CRDS and those of Roehl et al.[9] for $3\nu_{OH}$ also suggests that there may be uncertainty in the current literature cross sections for $2\nu_{OH}$, which are based on direct infrared absorption and action spectroscopy measurements.[8,9] Further measurements of the PNA overtone cross sections, in particular $2\nu_{OH}$, may therefore be of interest.

In a separate set of experiments, we have shown that HO_2 is produced from second overtone photodissociation of PNA and direct production of OH in this wavelength region in the atmosphere is negligible.

5. Conclusions

This paper presents measurements of spectra and band strengths for the second and third OH stretch overtone of PNA. The bands for the second and third overtone are symmetric without rotational structure centered at 10086.0 ± 0.2 and 13095.8 ± 0.4 cm^{-1}, with peak cross sections of $(8.8 \pm 1.7) \times 10^{-22}$ and $(7.0 \pm 1.3) \times 10^{-23}$ cm^2 molecule^{-1}, and full widths at half-maximum at 298 K of 48.4 ± 1.4 and 44.6 ± 0.6 cm^{-1}, respectively. The integrated band intensities obtained were $(5.7 \pm 1.1) \times 10^{-20}$ and $(4.9 \pm 0.9) \times 10^{-21}$ cm^2 molecule^{-1} cm^{-1}. We also measured a low temperature spectrum of the second overtone at 231 K. The band intensity was identical to the room temperature spectrum, while the peak narrowed and increased in height. The band intensities measured in this work are significantly larger (between 58% and 170%) than previous measurements and theoretical calculations. The reason for this discrepancy is not immediately apparent. Adoption of the cross sections from this work would increase total atmospheric photolysis rates by 11%, thereby influencing calculated HO_x levels in the upper atmosphere and in polar regions. Photolysis of PNA in the second overtone band showed that HO_2 was a photolysis product. We did not find any indication that OH is produced and were able to put an upper limit of 10% (2σ) on its yield relative to that of HO_2.

Acknowledgment. We are grateful to Steve Leone for his interest in and support of our work in atmospheric chemistry and for being a wonderful scientific colleague. A.R.R. is especially grateful for his friendship and long scientific association. This work was funded in part by NOAA's Climate Goal.

References and Notes

(1) Donaldson, D. J.; Frost, G. J.; Rosenlof, K. H.; Tuck, A. F.; Vaida, V. *Geophys. Res. Lett.* **1997**, *24*, 2651.

(2) Sander, S. P.; Friedl, R. R.; Golden, D. M.; Kurylo, M. J.; Moortgat, G. K.; Wine, P. H.; Ravishankara, A. R.; Kolb, C. E.; Molina, M. J.; Finlayson-Pitts, B. J.; Huie, R. E.; Orkin, V. L. JPL Publication 06−02 2006.

(3) Staikova, M.; Donaldson, A. J.; Francisco, J. S. *J. Phys. Chem. A* **2002**, *106*, 3023.

(4) Gierczak, T.; Jimenez, E.; Riffault, V.; Burkholder, J. B.; Ravishankara, A. R. *J. Phys. Chem. A* **2005**, *109*, 586.

(5) Jimenez, E.; Gierczak, T.; Stark, H.; Burkholder, J. B.; Ravishankara, A. R. *J. Phys. Chem. A* **2004**, *108*, 1139.

(6) Salawitch, R. J.; Wennberg, P. O.; Toon, G. C.; Sen, B.; Blavier, J. F. *Geophys. Res. Lett.* **2002**, 29.

(7) Crim, F. F. *Annu. Rev. Phys. Chem.* **1984**, *35*, 657.

(8) Zhang, H.; Roehl, C. M.; Sander, S. P.; Wennberg, P. O. *J. Geophys. Res.-Atmos.* **2000**, *105*, 14593.

(9) Roehl, C. M.; Nizkorodov, S. A.; Zhang, H.; Blake, G. A.; Wennberg, P. O. *J. Phys. Chem. A* **2002**, *106*, 3766.

(10) Matthews, J.; Sharma, R.; Sinha, A. *J. Phys. Chem. A* **2004**, *108*, 8134.

(11) Matthews, J.; Sinha, A.; Francisco, J. S. *J. Chem. Phys.* **2004**, *121*, 5720.

(12) Wennberg, P. O.; Salawitch, R. J.; Donaldson, D. J.; Hanisco, T. F.; Lanzendorf, E. J.; Perkins, K. K.; Lloyd, S. A.; Vaida, V.; Gao, R. S.; Hintsa, E. J.; Cohen, R. C.; Swartz, W. H.; Kusterer, T. L.; Anderson, D. E. *Geophys. Res. Lett.* **1999**, *26*, 1373.

(13) Evans, J. T.; Chipperfield, M. P.; Oelhaf, H.; Stowasser, M.; Wetzel, G. *Geophys. Res. Lett.* **2003**, 30.

(14) Kim, S.; Huey, L. G.; Stickel, R. E.; Tanner, D. J.; Crawford, J. H.; Olson, J. R.; Chen, G.; Brune, W. H.; Ren, X.; Lesher, R.; Wooldridge, P. J.; Bertram, T. H.; Perring, A.; Cohen, R. C.; Lefer, B. L.; Shetter, R. E.; Avery, M.; Diskin, G.; Sokolik, I. *J. Geophys. Res.-Atmos.* **2007**, 112.

(15) Singh, H. B.; Salas, L.; Herlth, D.; Kolyer, R.; Czech, E.; Avery, M.; Crawford, J. H.; Pierce, R. B.; Sachse, G. W.; Blake, D. R.; Cohen, R. C.; Bertram, T. H.; Perring, A.; Wooldridge, P. J.; Dibb, J.; Huey, G.; Hudman, R. C.; Turquety, S.; Emmons, L. K.; Flocke, F.; Tang, Y.; Carmichael, G. R.; Horowitz, L. W. *J. Geophys. Res.-Atmos.* **2007**, 112.

(16) Stiller, G. P.; von Clarmann, T.; Bruehl, C.; Fischer, H.; Funke, B.; Glatthor, N.; Grabowski, U.; Hopfner, M.; Jockel, P.; Kellmann, S.; Kiefer, M.; Linden, A.; Lopez-Puertas, M.; Tsidu, G. M.; Milz, M.; Steck, T.; Steil, B. *J. Geophys. Res.-Atmos.* **2007**, 112.

(17) Murphy, J. G.; Thornton, J. A.; Wooldridge, P. J.; Day, D. A.; Rosen, R. S.; Cantrell, C.; Shetter, R. E.; Lefer, B.; Cohen, R. C. *Atmos. Chem. Phys.* **2004**, *4*, 377.

(18) Slusher, D. L.; Huey, L. G.; Tanner, D. J.; Chen, G.; Davis, D. D.; Buhr, M.; Nowak, J. B.; Eisele, F. L.; Kosciuch, E.; Mauldin, R. L.; Lefer, B. L.; Shetter, R. E.; Dibb, J. E. *Geophys. Res. Lett.* **2002**, 29.

(19) Stroud, C.; Madronich, S.; Atlas, E.; Ridley, B.; Flocke, F.; Weinheimer, A.; Talbot, B.; Fried, A.; Wert, B.; Shetter, R.; Lefer, B.; Coffey, M.; Heikes, B.; Blake, D. *Atmos. Environ.* **2003**, *37*, 3351.

(20) Brown, S. S.; Wilson, R. W.; Ravishankara, A. R. *J. Phys. Chem.* **2000**, *104*, 4976.

(21) Aldener, M.; Brown, S. S.; Stark, H.; Daniel, J. S.; Ravishankara, A. R. *J. Mol. Spectrosc.* **2005**, *232*, 223.

(22) Rothman, L. S.; Barbe, A.; Benner, D. C.; Brown, L. R.; Camy-Peyret, C.; Carleer, M. R.; Chance, K.; Clerbaux, C.; Dana, V.; Devi, V. M.; Fayt, A.; Flaud, J. M.; Gamache, R. R.; Goldman, A.; Jacquemart, D.; Jucks, K. W.; Lafferty, W. J.; Mandin, J. Y.; Massie, S. T.; Nemtchinov, V.; Newnham, D. A.; Perrin, A.; Rinsland, C. P.; Schroeder, J.; Smith, K. M.; Smith, M. A. H.; Tang, K.; Toth, R. A.; Vander Auwera, J.; Varanasi, P.; Yoshino, K. *J. Quant. Spectrosc. Radiat. Transfer* **2003**, *82*, 5.

(23) Giver, L. P.; Valero, F. P. J.; Goorvitch, D. *J. Opt. Soc. Am. B* **1984**, *1*, 715.

(24) Klee, S.; Winnewisser, M.; Perrin, A.; Flaud, J. M. *J. Mol. Spectrosc.* **1999**, *195*, 154.

(25) Molina, L. T.; Molina, M. J. *J. Photochem.* **1981**, *15*, 97.

(26) Singer, R. J.; Crowley, J. N.; Burrow, J. P.; Schneider, W.; Moortgat, G. K. *J. Photochem. Photobiol.* **1989**, *48*, 17.

(27) Smith, C. A. *The atmospheric reaction kinetics of OH by flash-photolysis-resonance fluorescence. Thesis*; University of California: Berkeley, CA, 1983.

(28) Smith, C. A.; Molina, L. T.; Lamb, J. J.; Molina, M. J. *Int. J. Chem. Kinet.* **1984**, *16*, 41.

(29) Stutz, J.; Platt, U. *Appl. Opt.* **1996**, *35*, 6041.

(30) Kenley, R. A.; Trevor, P. L.; Lan, B. Y. *J. Am. Chem. Soc.* **1981**, *103*, 2206.

(31) Saxon, R. P.; Liu, B. *J. Phys. Chem.* **1985**, *89*, 1227.

(32) Suenram, R. D.; Lovas, F. J.; Pickett, H. M. *J. Mol. Spectrosc.* **1986**, *116*, 406.

(33) Chen, Z.; Hamilton, T. P. *J. Phys. Chem.* **1996**, *100*, 15731.

(34) Jitariu, L. C.; Hirst, D. M. *J. Phys. Chem. A* **1999**, *103*, 6673.

(35) May, R. D.; Friedl, R. R. *J. Quant. Spectrosc. Radiat. Transfer* **1993**, *50*, 257.

JP802259Z